RSC Advances

Volume 1 | Number 1 | Jan 2013 | Pages 1–100

RSC Advances

www.rsc.org/advances

ROYAL SOCIETY OF CHEMISTRY

This is an *Accepted Manuscript*, which has been through the Royal Society of Chemistry peer review process and has been accepted for publication.

Accepted Manuscripts are published online shortly after acceptance, before technical editing, formatting and proof reading. Using this free service, authors can make their results available to the community, in citable form, before we publish the edited article. This *Accepted Manuscript* will be replaced by the edited, formatted and paginated article as soon as this is available.

You can find more information about *Accepted Manuscripts* in the **Information for Authors**.

Please note that technical editing may introduce minor changes to the text and/or graphics, which may alter content. The journal's standard **Terms & Conditions** and the **Ethical guidelines** still apply. In no event shall the Royal Society of Chemistry be held responsible for any errors or omissions in this *Accepted Manuscript* or any consequences arising from the use of any information it contains.

ROYAL SOCIETY OF CHEMISTRY

www.rsc.org/advances

1

2

3

4

5 **Nanoparticle supported, magnetically separable manganese porphyrin as an**

6 **efficient retrievable nanocatalyst in hydrocarbon oxidation reactions**

7

8 Mojtaba Bagherzadeh[*] and Anahita Mortazavi-Manesh

9 *Chemistry Department, Sharif University of Technology, P.O. Box 11155-3615, Tehran, Iran.*

10

11

12

13

14

15

16

17

18

19

20

21

RSC Advances Accepted Manuscript

* Corresponding author. Tel.: +98 21 66165354; fax: +98 21 66012983;
*E-mail address:*bagherzadeh@sharif.edu

RSC Advances Accepted Manuscript

22　**Abstract**

23　A manganese porphyrin, *meso*-tetrakis(pentafluorophenyl)porphyrinato manganese (III) acetate,

24　Mn(TPFPP)OAc, was immobilized on silica-coated magnetic Fe_3O_4 nanoparticles which

25　functionalized with 3-aminopropyltriethoxysilane (APTS) through the amino propyl linkage

26　using a grafting process in toluene solvent. This enabled the covalent immobilization of Mn(III)

27　porphyrin via an aromatic nucleophilic substitution reaction, to afford the $Fe_3O_4@SiO_2$-

28　$NH_2@MnPor$ catalyst. The resulting nanoparticles were characterized by X-ray powder

29　diffraction (XRD), scanning electron microscopy (SEM), FT-IR spectroscopy, UV-Vis

30　spectroscopy, elemental analysis (CHN), atomic absorption spectroscopy (AAS), and vibrating

31　sample magnetometry (VSM). The immobilized manganese porphyrin was applied as an

32　efficient and retrievable heterogeneous nanocatalyst in the alkane hydroxylation and alkene

33　epoxidation. Leaching and recycling experiments revealed that the prepared nanocatalyst can be

34　recovered, and reused several times, without loss of activity and magnetic properties.

35　Keywords: Manganese porphyrin, Fe_3O_4 nanoparticle, Magnetically separable nanocatalyst,

36　Heterogeneous catalysis, Oxidation reactions

37　**1. Introduction**

38　Metalloporphyrins are well known to mimic the activity of enzymatic monooxygenases.[1,2] In this

39　regard, metalloporphyrin complexes have been largely employed as valuable biomimetic

40　catalysts, owing to the critical roles they play in oxygen transfer processes.[3] Investigating in this

41　area is based on different strategies to design selective, stable and high turnover catalytic

42　systems.[4,5] The introduction of second-generation metalloporphyrins, which bear bulky and/or

43　electron-withdrawing substituents at the *meso* positions of the porphyrin ring, has been among

44　the main approaches commonly employed with the aim of increasing the stability of the aromatic

45　heterocycle towards oxidative degradation in reaction condition. Immobilization of expensive

46　metalloporphyrin catalysts onto supports appears to be a good way to improve their oxidative

47　stability, selectivity and the catalytic performance because of the support environment and other

48　advantages with respect to recovery and reuse.[6-11] In other words, supporting metalloporphyrins

49　provides a physical separation of active sites, thus minimizing catalyst self-destruction and

50　metalloporphyrin dimerization.[10,12] Furthermore, heterogeneous catalytic oxidations have

51 become an important target since their process are used in industry, helping to minimize the

52 problems of industrial waste treatment. Hence, the immobilization of these biomimetic catalysts

53 is much desired.

54 An attractive approach is the preparation of magnetically separable nanocatalysts.[13-16] In this

55 manner, silica-coated magnetic nanoparticles, $Fe_3O_4@SiO_2$, have been studied extensively due to

56 their superparamagnetism property, large surface area to volume ratio and easy functionalization.

57 Homogeneous catalysts immobilized on magnetic nanoparticles (MNPs) surface occupy a unique

58 position due to combining the advantages of both homogeneous and heterogeneous catalysts.[17-19]

59 Because of large surface area of nanoparticles, high loadings of catalytically active sites are

60 guaranteed and therefore nanoparticles supported homogeneous catalysts exhibit high catalytic

61 activity and selectivity.[16] In addition, the magnetic properties of the Fe_3O_4 nanoparticles can

62 optimize the operations of separation, recycling, and reuse of the heterogeneous catalyst.[20]

63 Hence, these nanoparticles make catalyst recovery more practical and faster than conventional

64 separation methods also reduce solvent consumption. In this way, the important issue of favoring

65 the green chemistry strategy is also covered.[21]

66 In the present work, we describe the preparation of an efficient heterogeneous catalyst

67 synthesized by immobilizing manganese porphyrin on functionalized magnetic nanoparticles via

68 the amino propyl linkage. Also, the catalytic activity of the supported catalyst, $Fe_3O_4@SiO_2$-

69 $NH_2@MnPor$, has been investigated in hydrocarbon oxidation reactions as a recyclable and

70 sustainable nanocatalyst.

71 **2. Experimental**

72 **2.1. Materials and Methods**

73 All reagents and solvents were purchased from Merck, Fluka or Aldrich chemical companies.

74 Iodosylbenzene[22] and tetra-*n*-butylammonium hydrogen monopersulfate[23] were synthesized

75 according to the literature procedure.

76 Scanning electron microscopy (SEM) was carried out on Philips XL30. FT-IR spectra were

77 recorded as KBr pellets using ABB FT-IR spectrophotometer. Measures of pH were carried out

78 by Mettler Toledo S40 SevenMulti™ pH-meter. X-ray diffraction (XRD) pattern was obtained

79 by D4 ENDEAVOR diffractometer (Bruker AXS Inc.) with Cu Kα as a radiation source.

80 Elemental analyses (CHN) were performed using a Heraeus Elemental Analyzer. A Varian

81 (AA220) flame atomic absorption spectrometer (air/acetylene flame) was used for manganese

82 ion determinations. UV-Vis spectra were recorded with a Shimadzu UV-2100 spectrometer.

83 Magnetic measurement of materials was investigated with a vibrating sample magnetometer

84 VSM (Meghnatis Daghigh Kavir Company, Iran) at room temperature. Gas chromatographic

85 (GC) analyses were performed on an Agilent Technologies 6890 N, 19019 J-413 HP-5, capillary

86 60 m × 250 μm × 1μm. Brunauer–Emmett–Teller (BET) surface area of the catalyst was

87 measured by Belsorp mini II instrument at -196°C.

2.2. Porphyrin Synthesis and Metallation

89 Porphyrins are a group of heterocyclic macrocycle organic compounds. The porphyrin ring

90 structure is aromatic, with a total of 26 electrons in the conjugated system. Various analyses

91 illustrate that not all atoms of the ring are involved equally in the conjugation.[24] One result of

92 this large conjugated system is that porphyrin molecules typically have very intense absorption

93 bands in the visible region. Porphyrins bind metals to form metalloporphyrin complexes. In the

94 present work, the free base, *meso*-tetrakis(penta-flourophenyl)porphyrin ($H_2F_{20}TPP$ or

95 H_2TPFPP), was prepared[25] and metallated with $Mn(OAc)_2 \cdot 4H_2O$ to afford the metalloporphyrin

96 [Mn(TPFPP)OAc].[26] The UV–Vis spectrum of homogeneous Mn(TPFPP)OAc was shown in the

97 Supplementary Information labeled as Fig. S1.

2.3. Preparation of Fe₃O₄ Magnetic Nanoparticles

99 Fe_3O_4 nanoparticles were synthesized on the basis of the procedure described previously.[19,27,28]

100 In brief, under N_2 atmosphere, 5.2 g (19.3 mmol) of $FeCl_3.6H_2O$, 2 g (10.0 mmol) of $FeCl_2.4H_2O$

101 and 0.85 mL concentrated HCl were dissolved in 25 mL degassed water. This solution was

102 added dropwise at room temperature to 250 mL of NaOH solution (1.5 mol/L) under N_2. The

103 reaction mixture was vigorously stirred for 30 min (1300 rpm). The formed black precipitates

104 were separated using a strong magnetic field (0.5 T magnet) and washed several times with

105 degassed water. Finally, for storage, Fe_3O_4 nanoparticles were dispersed in 200 mL degassed

106 water under N_2. Synthesis of Fe_3O_4 nanoparticles was approved by XRD.

107

2.4. Synthesis of Fe₃O₄@SiO₂ Nanoparticles

108

109　In the next step, Fe₃O₄MNPs were coated with a thin layer of silica.[19,29] One gram of freshly

110　prepared Fe₃O₄ nanoparticles was added into 30 mL of an aqueous solution of citric acid (0.02

111　g/mL), then the pH was adjusted to 5.2 using ammonia, and the mixture was heated to 80–90 °C

112　for 1.5 h. After heating, the pH of the reaction mixture was increased with ammonia to pH=11

113　and 1.25 mL of tetraethylorthosilicate (TEOS) dissolved in ethanol (12.5 mL) was added

114　dropwise into the suspension of particles. The mixture was stirred at room temperature for 24 h

115　to allow the base-catalyzed hydrolysis and condensation of TEOS monomers on the nanoparticle

116　surface go to completion. Finally, the dark brown Fe₃O₄@SiO₂ nanoparticles were separated

117　using a 0.5 T magnet and were washed with distilled water and ethanol. Synthesis of

118　Fe₃O₄@SiO₂ nanoparticles was confirmed with X-ray diffraction analysis.

2.5. Synthesis of Fe₃O₄@SiO₂-NH₂

119

120　In a typical reaction, 5 mL of 3-aminopropyltriethoxysilane (APTS) dissolved in 100 mL ethanol

121　were added dropewise to the suspension of one gram of the silica-coated Fe₃O₄ nanoparticles in

122　100 mL of distilled water. The pH value of the reaction mixture was increased with KOH to

123　pH=11 and the reaction mixture was stirred at 70 °C for five hours.[15,30] Finally, the brown

124　precipitates were separated using a 0.5 T magnet and were thoroughly washed with distilled

125　water to remove any unbound APTS. Functionalization of Fe₃O₄@SiO₂ nanoparticles was

126　confirmed by FT-IR spectroscopy, and elemental analysis (CHN).

2.6. Synthesis of Fe₃O₄@SiO₂-NH₂@MnPor Nanocatalyst

127

128　The process of manganese porphyrin immobilization was conducted by dispersing the

129　synthesized Fe₃O₄@SiO₂-NH₂ (0.10 g) in 10 mL of toluene, containing 4.6×10^{-5} mol of

130　metalloporphyrin. The suspension was refluxed and stirred for 24 h under argon atmosphere. The

131　solid was filtered, washed with toluene, CH₂Cl₂ and ethanol and dried at 60 °C overnight.[31,32]

132　The quantity of immobilized manganese porphyrin was determined by measuring the manganese

133　content of the prepared catalyst; Fe₃O₄@SiO₂-NH₂@[Mn(TPFPP)OAc], by atomic absorption

134　spectroscopy (AAS).

135

2.7. General Oxidation Procedure

A typical oxidation reaction using the $Fe_3O_4@SiO_2$-NH_2@[Mn(TPFPP)OAc] nanoparticles as catalyst is described as follows. In a 10 mL round-bottom flask, the prepared catalyst (0.01 g, containing 8×10^{-4} mmol of MnPor), the nitrogenous base of imidazole as the co-catalyst (0.064 mmol), substrate (0.2 mmol) and oxidant (0.4 mmol) were added in order with a molar ratio of {catalyst/imidazole/substrate/oxidant}:{1/80/250/500}. The reaction mixture was stirred at room temperature in a tightly closed flask. The progress of the reaction was monitored in different time intervals using gas chromatography (GC). The catalyst nanoparticles were collected at the bottom of the round-bottom flask using a magnet, supernatant carefully decanted and formation of products was examined by GC. The oxidation products were identified by comparison with authentic samples. An internal standard method was used to calculate yields. In the GC experiments, *n*-decane was used as the internal standard.

2.8. Reusability of the Catalyst

The reusability and the stability of the catalyst were studied in repeated oxidation reactions. At the end of each reaction, the catalyst was magnetically separated from the reaction mixture, washed with CH_2Cl_2 and then dried in vacuum at room temperature for 4 h before reusing in the subsequent oxidation reaction. The catalyst was consecutively reused about six times without detectable catalyst leaching or significant loss of activity.

3. Results & Discussion

As illustrated in Scheme 1, magnetically separable $Fe_3O_4@SiO_2$-NH_2@[Mn(TPFPP)OAc] (**1**) nanocatalyst was synthesized by multistep procedure. First, superparamagnetic Fe_3O_4 nanoparticles were prepared using the co-precipitation method. The synthesis of Fe_3O_4 nanoparticles was followed by coating the surface with a thin silica layer in order to increase the functionality and stability of nanoparticles. For this purpose, the silica-coated MNPs were obtained by basic hydrolysis and condensation of TEOS on the surface of the Fe_3O_4 nanoparticles. In the next step, $Fe_3O_4@SiO_2$ nanoparticles have been surface-modified with 3-aminopropyltriethoxysilane (APTS) which introduced -NH_2 group on to the surface of support. Eventually, the supported catalyst (**1**), was prepared by the reaction of $Fe_3O_4@SiO_2$-NH_2 with Mn(TPFPP)OAc. By the procedure of modification of Fe_3O_4 nanoparticles surface, covalent

165   bonding is a possible approach for this immobilization, because the manganese porphyrin

166   presents the pentafluorophenyl groups at the *meso*-positioned porphyrin ring, which can be

167   bonded to the functionalized silica by nucleophilic aromatic substitution. This mechanism is

168   described by the reaction of fluorine atoms from the *meso* porphyrin groups and pendant amino

169   groups from the $Fe_3O_4@SiO_2$ nanoparticles surface.[11,32,33]

170

171
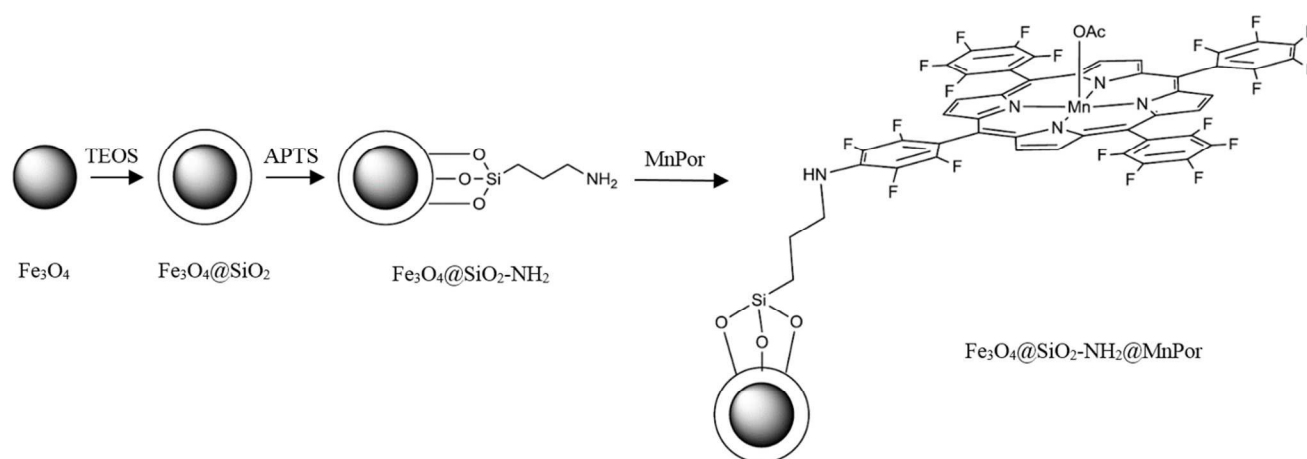
172   **Scheme 1.** Step-by-step synthesis of the nanocatalyst (**1**)

173   ### 3.1. Characterization of the Catalyst, $Fe_3O_4@SiO_2-NH_2@[Mn(TPFPP)OAc]$

174   Fig. 1 shows the XRD patterns of the synthesized compounds as they are shown schematically in

175   Scheme 1. The X-ray diffraction analysis was carried out for the nanoparticles before and after

176   growing a SiO_2 shell and after immobilization of the catalyst. In the XRD pattern of the prepared

177   Fe_3O_4, six characteristic peaks (2θ = 30.6, 35.7, 43.8, 54.2, 57.3, and 63.6), corresponding to

178   (220), (311), (400), (422), (511), and (440) Bragg reflections, respectively, were observed (Fig.

179   1a). These diffraction peaks are in good agreement with the database in JCPDS file (PCPDFWIN

180   v.2.02, PDF No. 85-1436) and reveal that the resultant nanoparticles were pure Fe_3O_4 without

181   impurity phases. This XRD pattern is consistent with the pattern previously reported for Fe_3O_4

182   samples.[19,34] The XRD pattern of $Fe_3O_4@SiO_2$ core/shell is shown in Fig. 1b. The same

183   characteristic peaks can also be found in this pattern indicating that the crystalline structure of

184   Fe_3O_4 nanoparticles did not change after the surface modification with silica. The weaker peaks

185   intensity in pattern of Fig. 1b than that of Fig. 1a can be attributed the shielding effect of

186   amorphous silica shell. Also, Fig. 1 shows the XRD patterns of the MNPs-NH_2 and MNPs-

187   NH_2@MnPor (Fig. 1c, 1d) with specific peaks and relative intensity, which completely match

188   with the standard Fe_3O_4 sample.

189
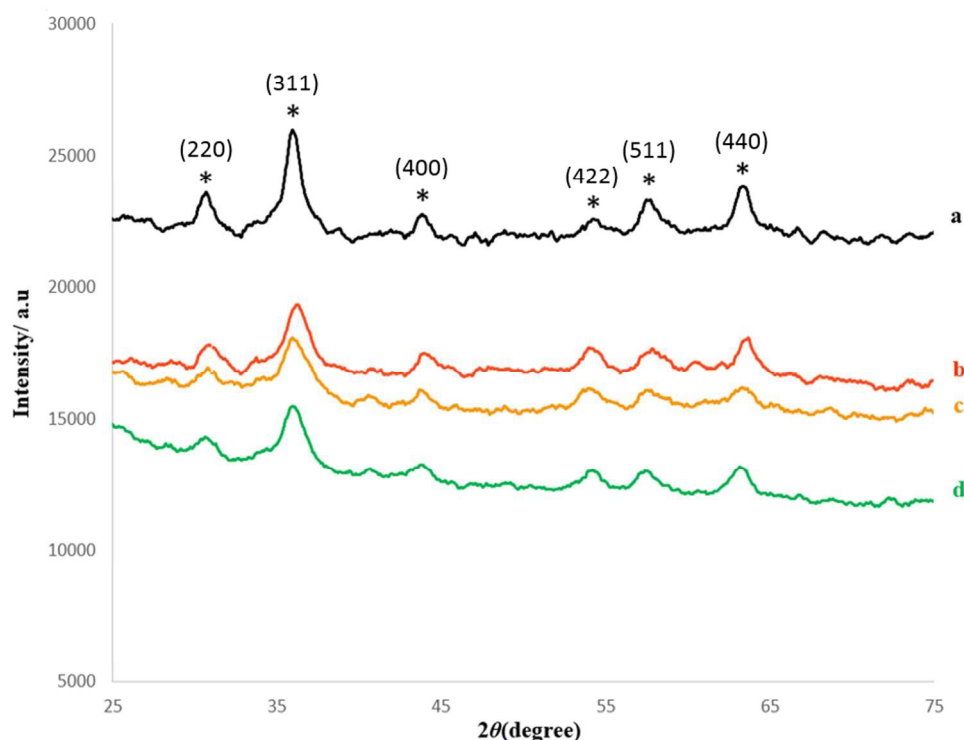
190

191   **Fig. 1.** XRD pattern of: (a) Fe_3O_4, (b) Fe_3O_4@SiO_2 (c) Fe_3O_4@SiO_2-NH_2 (d) Fe_3O_4@SiO_2-NH_2@MnPor

192   Scanning electron microscopy (SEM) image of Fe_3O_4@SiO_2-NH_2@[Mn(TPFPP)OAc] catalyst

193   clearly depicts a smooth morphology of the nanocatalyst; particles were well distributed with

194   diameters around 27 nm and rather high surface area (Fig. 2). Brunauer–Emmett–Teller (BET)

195   analysis of the nanocatalyst was performed and the obtained N_2 adsorption–desorption isotherm

196   is depicted in Fig. S2. which is located in Supplementary Information. The BET analysis is the

197   most common method for determining surface areas from nitrogen adsorption isotherms.[35] The

198   measured BET surface area is 81.2 m^2 g^{-1} for the nanocatalyst (**1**). Therefore, the relatively high

199   surface area of nanoparticles is beneficial for high loading of catalyst during the complex
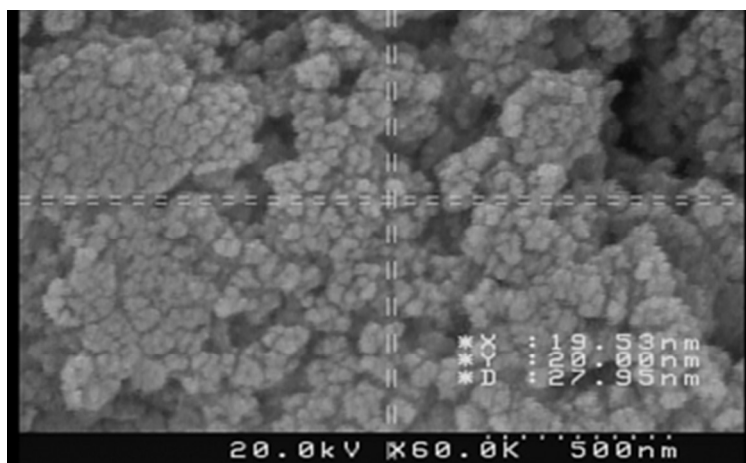
200   anchoring step.

RSC Advances Accepted Manuscript

201

202   **Fig. 2.** The scanning electron microscopy image of $Fe_3O_4@SiO_2-NH_2@[Mn(TPFPP)OAc]$

203   Because of the presence of the magnetic core inside, MNPs cannot be analyzed by means of

204   solid state NMR spectroscopy. Therefore amino functionalized nanoparticles ($Fe_3O_4@SiO_2-NH_2$)

205   were systematically characterized by FT-IR and elemental analysis. Fig. 3 shows the FT-IR

206   spectra of the core-shell magnetic nanoparticles ($Fe_3O_4@SiO_2$) after being functionalized by

207   APTS. The FT-IR spectrum (Fig. 3a) represents significant absorption bands at about 586 and

208   632 cm^{-1} which corresponds to Fe–O vibration modes of Fe_3O_4. Furthermore, a strong absorption

209   band at around 1068 cm^{-1} (between 1000 and 1200 cm^{-1}) and a band at 794 cm^{-1}, which can be

210   assigned as vibration modes of Si–O–Si,[36,37] indicate that the Fe_3O_4 core is successfully coated

211   by silica shell. Another bands at around 1622 and 3427 cm^{-1} are associated with the vibrations of

212   absorbed water molecules.[38]

213   Additionally, the characteristic peaks at 2854 and 2923 cm^{-1} ascribed to the C-H stretching

214   vibration of the propyl group in the pendant APTS can be clearly observed in the FT-IR

215   spectrum of $Fe_3O_4@SiO_2-NH_2$, which confirms that APTS molecules have been bonded

216   successfully to the surface of the silica-coated MNPs.[39] This conclusion is further supported by

217   the elemental analysis which gave the percentages of C, H, and N to be 5.10%, 1.54%, and

218   1.53%, respectively. The frequency of N-H asymmetric and symmetric stretching vibrations of

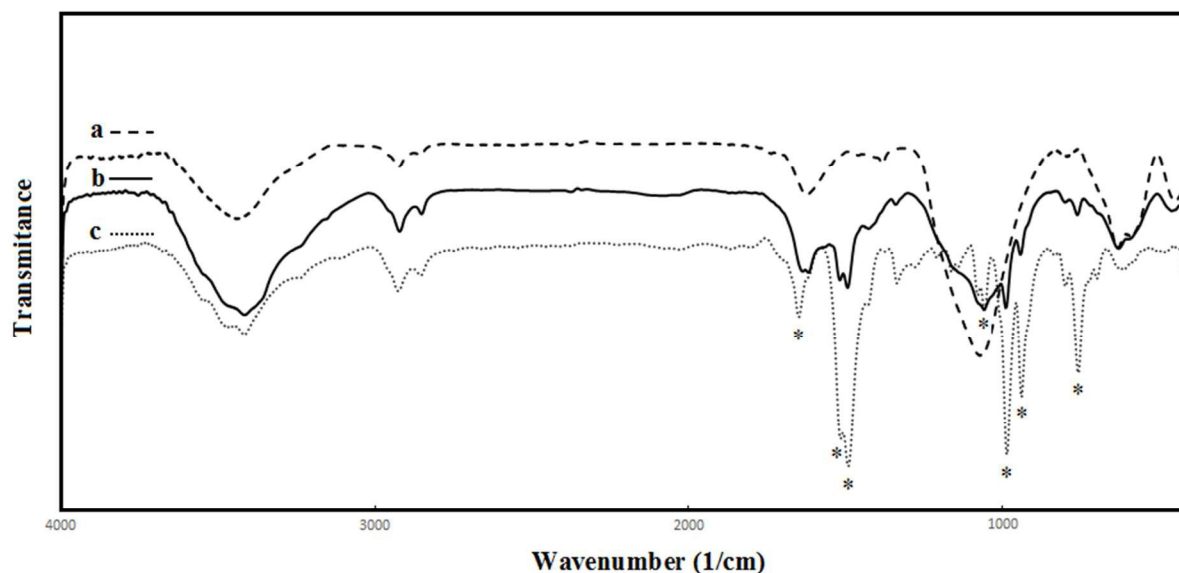219   the amine group fall in the 3300-3400 cm^{-1} range and are obscured by the water band.

220

221   Fig. 3. FT-IR spectra of: (a) $Fe_3O_4@SiO_2-NH_2$ (b) $Fe_3O_4@SiO_2-NH_2@[Mn(TPFPP)OAc]$, (c) $Mn(TPFPP)OAc$

222   Furthermore, immobilization of metalloporphyrin on APTS-coated magnetic nanoparticles was

223   exhibited by FT-IR spectroscopy. Comparing FT-IR spectra of $Fe_3O_4@SiO_2-NH_2@MnPor$ (Fig.

224   3b) and Mn-porphyrin (Fig. 3c) revealed that signals at about 759, 941, 987, 1492, 1517 and

225   1649 cm^{-1} corresponding to the vibration modes of pure metalloporphyrin are present in the FT-

226   IR spectra of $Fe_3O_4@SiO_2-NH_2@[Mn(TPFPP)OAc]$ nanoparticles. The loading of manganese

227   porphyrin complex was 0.08 mmol/g of the supported nanocatalyst, determined by AAS

228   analysis.

229   The presence of MnPor on functionalized magnetic nanoparticles was analyzed by means of

230   UV–Vis spectroscopy (Fig.4). No absorption band was observed in the UV–Vis spectra of

231    $Fe_3O_4@SiO_2-NH_2$ (Fig.4b, dash line). However, the Soret and Q bands at 475 and 576 nm

232   respectively were appeared after immobilization process of $Mn(TPFPP)OAc$ on the surface (Fig.

233   4a). In this way, both of the FT-IR and UV-Vis spectroscopy provide evidences for anchoring of

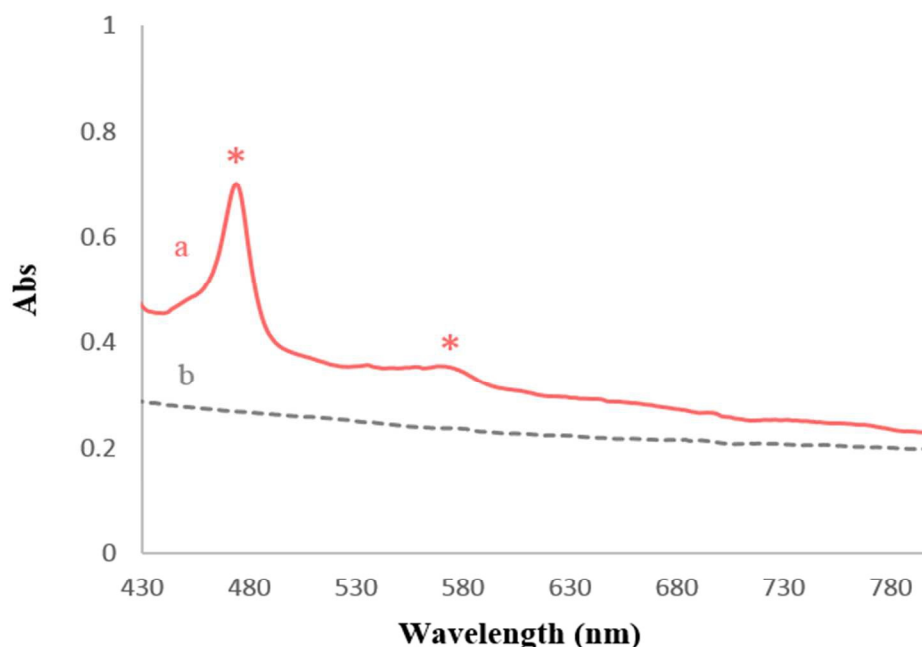234   the manganese porphyrin on APTS-coated Fe_3O_4 NPs.

RSC Advances Accepted Manuscript

235

236   **Fig. 4.** UV–Vis spectra of: (a) $Fe_3O_4@SiO_2-NH_2$, (b) $Fe_3O_4@SiO_2-NH_2@[Mn(TPFPP)OAc]$

237   The magnetic properties of uncoated Fe_3O_4 nanoparticles, $Fe_3O_4@SiO_2$, and the $Fe_3O_4@SiO_2$-

238    $NH_2@[Mn(TPFPP)OAc]$ catalyst were characterized by a vibrating sample magnetometer

239   (VSM) under an applied field of -10 000 to 10 000 Oe at room temperature (Fig. 5). According

240   to the magnetization curves, the reduced saturation magnetization values observed for the

241   functionalized nanoparticles (Fig. 5b, 5c) as compared with pure Fe_3O_4 nanoparticles (Fig. 5a)

242   were due to the diamagnetic surface coating and surface functionalization of Fe_3O_4

243   nanoparticles.[40,41] However, both in the case of the core-shell MNPs and of the final

244   nanocatalyst, such values are still large enough for nanoparticles to be easily separated by an
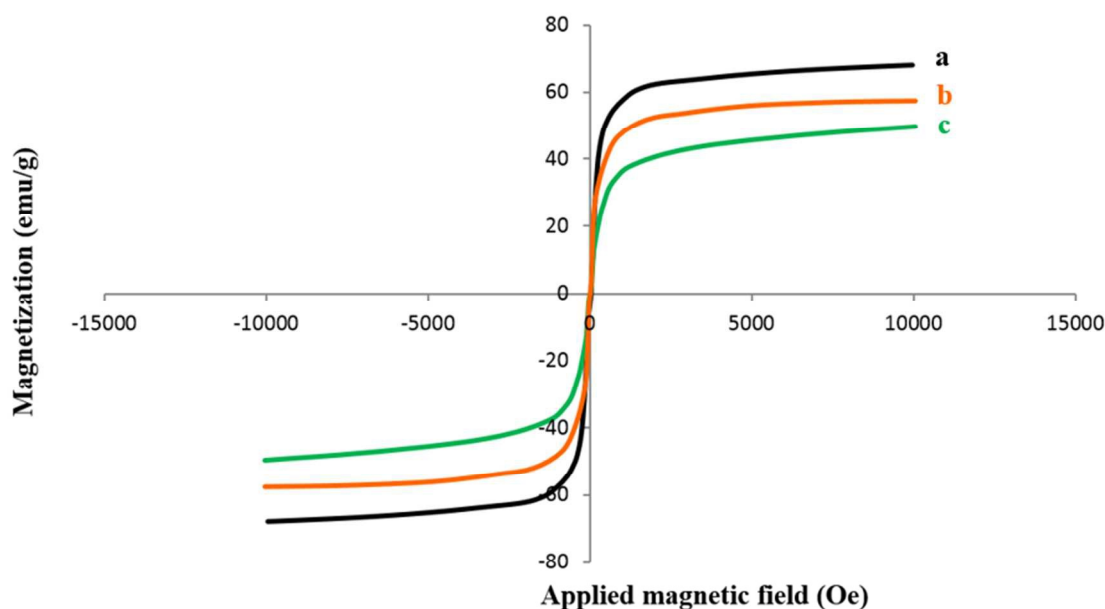
245   external magnet.

246

247   **Fig. 5.** Magnetization curves of: (a) Fe_3O_4 (b)$Fe_3O_4@SiO_2$ (c) $Fe_3O_4@SiO_2$-NH_2@[Mn(TPFPP)OAc]

248

249   **3.3. Catalytic Experiments**

250   The present work reports the catalytic activity of Mn(TPFPP)OAc supported on APTS-coated

251    $Fe_3O_4@SiO_2$ nanoparticles; $Fe_3O_4@SiO_2$-NH_2@[Mn(TPFPP)OAc] (**1**), in alkane oxidation in

252   the presence of two different oxidants; tetra-*n*-butylammonium hydrogen monopersulfate (*n*-

253   Bu_4NHSO_5) and iodosylbenzene (PhIO). Catalytic performance of heterogeneous catalyst (**1**) in

254   alkene epoxidation with *n*-Bu_4NHSO_5 was also investigated as shown in Scheme 2.

255
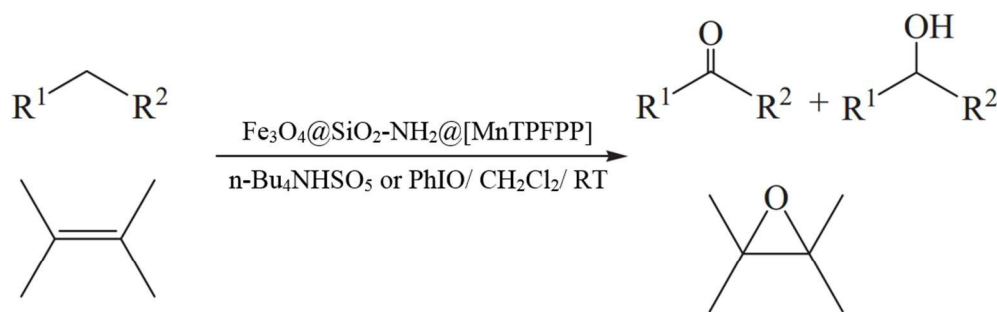
256   **Scheme 2.** Hydroxylation of alkanes and epoxidation of alkenes catalyzed by $Fe_3O_4@SiO_2$-NH_2@[MnTPFPP] (**1**)

257   It is believed that the employment of imidazoles in metalloporphyrin systems for mimicking the

258   axial coordination function of cytochrome-P450 has led to remarkable improvement in oxidation

259   reactions.[42,43] According to the co-catalytic role of axial base in biomimetic oxidations catalyzed

260   with manganese porphyrins,[44,45] imidazole nitrogenous base was employed as axial ligand in the

261   mentioned reactions. Imidazole with the ability of σ-donating and π-donating, mainly exhibited

262   higher activity as a co-catalyst, compared to other nitrogenous bases.

263   The   oxidation   reactions   were   carried   out   with   molar   ratio   of

264   {catalyst/imidazole/substrate/oxidant}:{1/80/250/500} at room temperature in CH_2Cl_2 as the

265   reaction medium.

266   **3.3.1**. **Alkane Hydroxylation catalyzed by $Fe_3O_4@SiO_2$-NH_2@[Mn(TPFPP)OAc]**

267   One of the typical challenging areas in organic chemistry is the catalytic oxidation of saturated

268   hydrocarbons under mild conditions.[46,47] For this purpose the catalytic performance of

269   $Fe_3O_4@SiO_2$-NH_2@[Mn(TPFPP)OAc] was investigated in biomimetic oxidation of alkanes (Fig.

270   6). In order to find the suitable reaction conditions, the ability of two different single oxygen

271   donors such as tetra-n-butylammonium hydrogen monopersulfate (n-Bu_4NHSO_5) and

272   iodosylbenzene (PhIO) was examined in the oxidation of alkanes in dichloromethane medium

273   after 4 h. The results, which are summarized in Fig. 6, show that n-Bu_4NHSO_5 gives the higher

274   oxidation conversion. This observation could be explained based on the ability of hydrogen

275   bonding formation between the *ortho*-C–F groups of MnPor with the hydrogen of oxidant in case
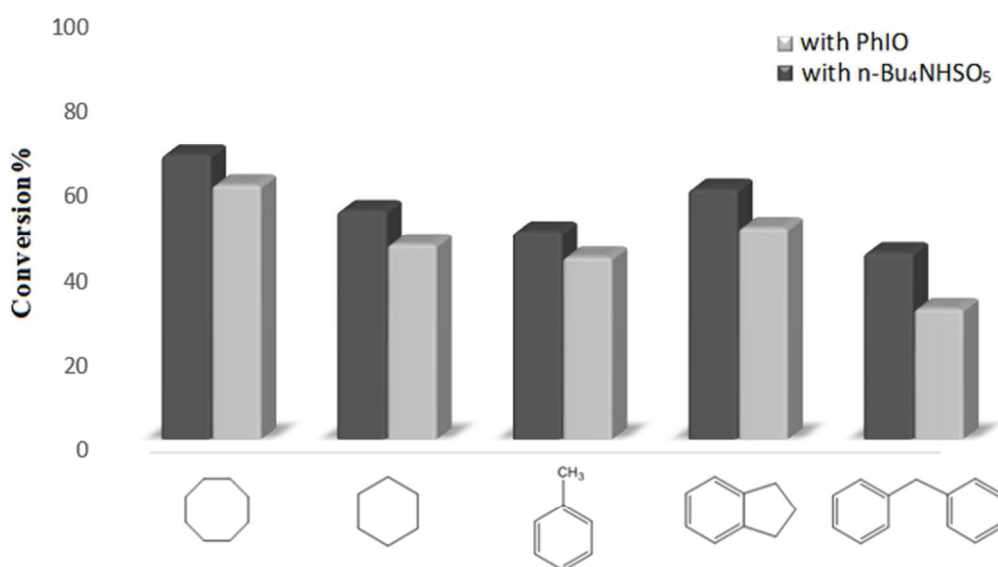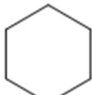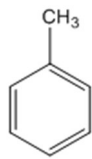
276   of n-Bu_4NHSO_5.

277

278
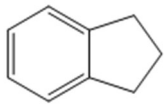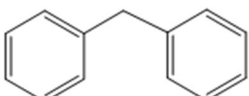
Fig. 6. Oxidation of alkanes catalyzed by $Fe_3O_4@SiO_2-NH_2@[Mn(TPFPP)OAc]$ in the presence of two different oxidants: $n\text{-Bu}_4NHSO_5$ and PhIO.

This heterogenized catalytic system converts different alkanes to their corresponding alcohols and aldehyde/ketones (Table 1). The oxidation of cyclooctane, cyclohexane, toluene, indane and diphenylmethane in dichloromethane solution at room temperature catalyzed by immobilized Mn-porphyrin gives respectively cyclooctanone, cyclohexanone, benzaldehyde, 1-indanone and benzophenone as the main product, as well as smaller amounts of cyclooctanol, cyclohexanol, benzyl alcohol and 1-indanol. In addition; to study the influence of time in the oxidation process, the reactions were carried out in two different time intervals. It can be observed that $Fe_3O_4@SiO_2-NH_2@[Mn(TPFPP)OAc]$ is an efficient catalyst for oxidation of alkanes in the presence of $n\text{-Bu}_4NHSO_5$. Therefore, the results of this study show better catalytic performance of the heterogonous catalyst using $n\text{-Bu}_4NHSO_5$ as oxidant in comparison with PhIO in oxidation reactions both in terms of selectivity and conversion levels.

296   **Table 1.** Hydroxylation of alkanes catalyzed by $Fe_3O_4@SiO_2-NH_2@[MnTPFPP]^a$

Entry	Alkane	Conversion%[a,b]	Selectivity to aldehyde/ketone%[e]	TON[f]
1		71 (67)[c] [64 (60)[c]][d]	62 [60][d]	177.5
2		55 (54)[c] [48 (46)[c]][d]	80 [76][d]	137.5
3	CH3	52 (49)[c] [44 (43)[c]][d]	95 [89][d]	130
4		65 (59)[c] [57 (50)[c]][d]	73 [70][d]	162.5
5		47 (44)[c] [36 (31)[c]][d]	100 [100][d]	117.5

297   [a]Reaction conditions: alkane (0.2 mmol), n-Bu$_4$NHSO$_5$ (0.4 mmol), catalyst (8×10^{-4} mmol), CH_2Cl_2 (1 mL), Reaction time:
298   20 h. [b]Determined by GC. [c]Values in parentheses were obtained after 4 h. [d]Values in brackets were obtained in the presence
299   of PhIO. [e]Selectivity to (aldehyde/ketone) = ((aldehyde/ketone)/((aldehyde/ketone) + alcohol)) × 100. [f]TON = (mmol of
300   product)/mmol of catalyst.

301

302   A cage-controlled radical mechanism, the "oxygen rebound" mechanism, has been proposed and

303   discussed for the manganese(III) porphyrin-catalyzed hydroxylation of alkanes.[48-50] This process

304   involves two steps: firstly, hydrogen atom abstraction by the active specie $Mn^V(O)P$ generates a

305   solvent-caged alkyl radical and a hydoxymanganese(IV) species (Scheme 3, pathway A); in the

306   second step, a subsequent 'in cage' reaction leads to the formation of the alcohol and the MnPor

307   is recovered. However, in competition with the second step, the carbon radicals can escape from

308   the cage (Scheme 3, pathway B), thus triggering radical processes, with the production of ketone

309   products.[51,52]
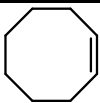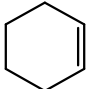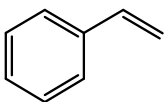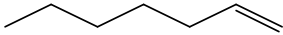
310
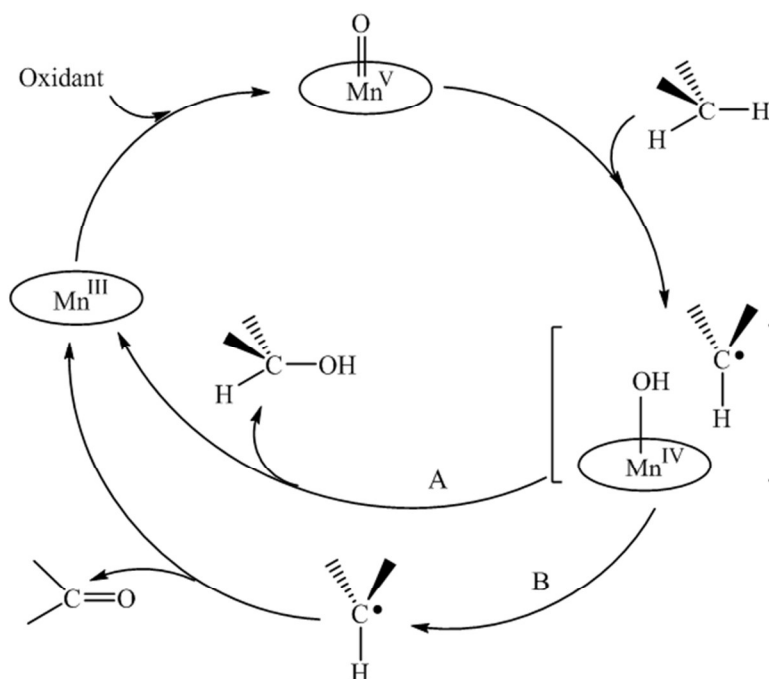
311   **Scheme 3.** Mechanism of the MnPor-catalyzed oxidation of alkanes

312   **3.3.2. Alkene epoxidation catalyzed by $Fe_3O_4@SiO_2$-$NH_2@[Mn(TPFPP)OAc]$**

313   Catalytic oxidation of olefins constitutes an important area in modern chemistry.[53-56] The

314   transition metal-catalyzed epoxidation reaction provides a convenient route for preparing

315   epoxides. In this regard, the $Fe_3O_4@SiO_2$-$NH_2@[Mn(TPFPP)OAc]$ was used as an efficient

316   catalyst for the epoxidation of alkenes with n-Bu_4NHSO_5 in CH_2Cl_2 as a solvent (Table 2). This

317   catalytic system showed high activity in the oxidation of cyclooctene and afforded the

318   cyclooctene oxide in 97% after 20 h. In the case of cyclohexene, the major product was

319   cyclohexene oxide (88%) and 2-cyclohexen-1-one was produced as a minor product (5%).

320   Epoxidation of styrene yielded 94% of styrene oxide with only a small amount of benzaldehyde

321   as by-product after 20 h. The epoxidation of linear alkenes such as 1-heptene and 1-octene was

322   also investigated. Linear alkenes which have the lowest electron densities and no conjugated π-

323   bondings are less reactive than cyclic ones. The best conversion was obtained after 20 h in terms

324   of calculated turnover numbers (TON) as shown in Table 2.

325

326

327   **Table 2.** Epoxidation of alkenes with n-Bu$_4$NHSO$_5$ catalyzed by Fe$_3$O$_4$@SiO$_2$-NH$_2$@[MnTPFPP][a]

Entry	Alkene	Conversion% [a,b]	Selectivity to epoxide%	TON[f]
1		97 (85)[c]	100	242.5
2		93[d] (83)[c,d]	94	232.5
3		94[e] (81)[c,e]	92	235
4		48 (37)[c]	100	120
5		56 (43)[c]	100	140

328   [a]Reaction conditions: alkene (0.2 mmol), n-Bu$_4$NHSO$_5$ (0.4 mmol), catalyst (8×10^{-4} mmol), CH$_2$Cl$_2$ (1 mL),
329   Reaction time: 20 h. [b]Determined by GC. [c]Values in parentheses were obtained after 3 h. [d]The by-product is allylic
330   ketone. [e]The by-product is benzaldehyde. [f]TON = (mmol of product)/mmol of catalyst.

331   For alkene epoxidation, there are some mechanism reports of parallel reactions occurring besides

332   the concerted epoxidation mechanism (Scheme 4, pathway A). In these mechanisms, the active

333   specie Mn^V(O)P forms a charge transfer complex with the alkene.[1,57-59] As shown in Scheme 4,

334   two processes can occur: (B) the charge transfer complex generates a radical intermediate, that

335   will attack the alkene generating the epoxidized product, or (C) the charge transfer complex

336   generates a solvent-caged alkyl radical, which favors the electron transfer from the alkene to the

337   Mn^V(O)P, followed by the formation of a carbocation and subsequent oxygen transfer, thus

338   generating the epoxidized product.[48,60] It should be mentioned whenever the reaction goes

339   through each of the radical pathways (B and/or C), a variety of products may be readily yielded.

340   According to the negligible difference of conversion and epoxidation yield as shown in Table 2,

341   epoxide seems to be the sole main product. Therefore a concerted mechanism (pathway A) may

342   play a role here for the reaction progress.
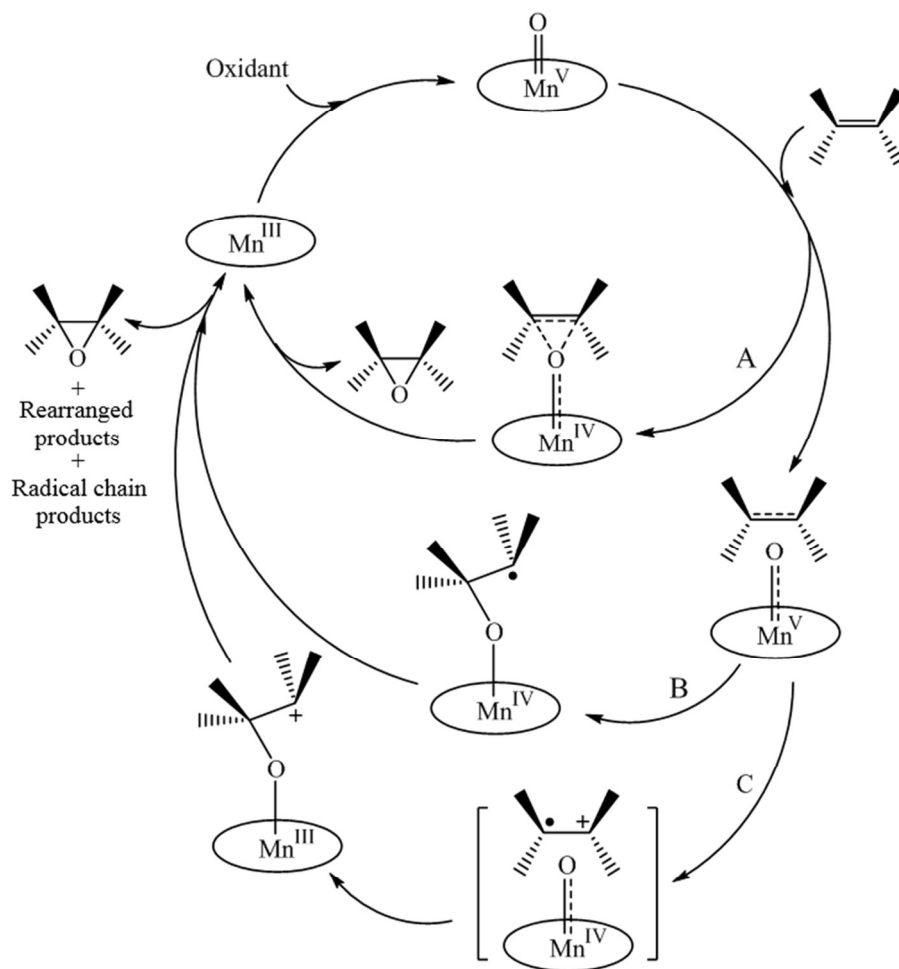
Scheme 4. Mechanism of the MnPor-catalyzed oxidation of alkenes

3.3.3. Catalyst Reuse and Stability

The reusability of a heterogeneous catalyst is of prime importance in catalyst design. Under homogeneous conditions, manganese porphyrin cannot be recovered even once but the nanomagnet-immobilized Mn-porphyrin can be magnetically separated and reused multiple times without detectable catalyst leaching or significant loss of catalytic activity. In this manner, for completion of our study, the reusability of the prepared catalyst, $Fe_3O_4@SiO_2$-$NH_2@[Mn(TPFPP)OAc]$, was checked in the multiple sequential epoxidation of cyclooctene with n-Bu_4NHSO_5. The catalyst was separated from the reaction mixture after each run using a magnet, washed with CH_2Cl_2 and dried before being used again. As shown in Table 3, the catalyst could be reused for six consecutive times without significant loss of its catalytic activity. Also, the filtrates were collected and the amounts of Mn leached after each run were determined

356   by AAS analysis. As illustrated in Table 3, small amounts of manganese were detected in the

357   filtrates.

358   **Table 3.** The results of catalyst recovery in the epoxidation of cyclooctene

Run	Conversion% [a]	Mn leached% [a,b]
1	97	1.4 (0.06)[d]
2	92	0.8 (0.03)[d]
3	89	0.5 (0.02)[d]
4	88	c
5	87	c
6	87	c

359   [a]Reaction conditions: cyclooctene (0.2 mmol), n-Bu$_4$NHSO$_5$ (0.4 mmol), CH$_2$Cl$_2$ (1
360   mL), Reaction time: 20 h. [b]Determined by AAS. [c]Not detected. [d]Values in parentheses
361   were reported in ppm.

362   Comparison of the catalytic performances presented in this work with those of other similar

363   studies[61-67] reveals that our catalytic system is superior to some of the previously reported

364   catalysts in terms of catalytic activity (TON) and reaction conditions. The high turnover number

365   of our catalyst compared to recently reported protocols[61,62] makes the Fe$_3$O$_4$@SiO$_2$-

366   NH$_2$@[MnTPFPP] more attractive for oxidation of hydrocarbons. In other words, compared with

367   these nonporphyrin catalysts, our catalytic system exhibits high catalytic activity in term of high

368   TON. According to the molar ratio of 1/250/500 for catalyst/substrate/oxidant which is carried

369   out in this work, the amount of catalyst which is used in each run (0.01 g, containing 8×10^{-4}

370   mmol of MnPor) is lower than that of previous works.[61-66]

371   It is observed that in several articles,[62,65] performance of the catalyst in oxidation of various

372   substrates was inspected under reflux, while the oxidation reactions were carried out at room

373   temperature in this work. It should be mentioned that the insertion of an oxygen atom within the

374   C−H of a saturated carbon atom is one of the most difficult reactions to achieve with a catalyst at

375   room temperature.

376   Our heterogenized catalytic system, can be recovered and reused in comparison with the

377   homogeneous complexes.[61-64] Metal complexes are stabilized upon immobilization on solid

378   supports because of the support environment. Also, the formation of inactive dimer, the major

379 drawback of homogeneous catalyst, is prevented by site isolation on the surface. Moreover, non-

380 magnetic heterogeneous systems[66,67] require filtration and centrifugation steps to recover the

381 catalysts leading to loss of catalytic activity during consecutive cycles. Therefore, the

382 magnetically supported nanocatalyst, the present work, can be conveniently separated from

383 reaction solution with a magnet and reused several times without significant loss of activity.

384 **4. Conclusions**

385 This work describes the covalent immobilization of Mn-porphyrin, 5,10,15,20-

386 tetrakis(pentafluorophenyl)porphyrin manganese(III) acetate Mn(TPFPP)OAc, onto magnetic

387 nanoparticles covered with amino functionalized silica. This magnetically separable

388 metalloporphyrin was applied as an efficient retrievable heterogeneous nanocatalyst for the

389 oxidation of a variety of alkanes and alkenes. In other words, this heterogenized catalytic system

390 could join the catalytic properties of the manganese porphyrin with the magnetic properties of

391 Fe_3O_4 nanoparticles. The results show that the dispersion of these superparamagnetic

392 nanoparticles, which can be reversibly controlled by applying an external magnetic field,

393 introducing them as the recyclable support matrix in the catalytic oxidations. Because of the

394 relatively high surface area of these nanoparticles, high loadings of catalytically active sites are

395 guaranteed and therefore high catalytic activity is provided for the supported metalloporphyrin

396 catalyst.

397 Furthermore, the separation and reuse of the magnetic Fe_3O_4 nanoparticles were very effective

398 and economical. Leaching and recycling experiments revealed that nanocatalyst is already

399 recyclable several times without loss of activity and magnetic properties. The attractive features

400 of this catalytic system such as easy work up, noticeable reusability and mild reaction conditions

401 make it particularly suitable for hydrocarbon oxidation reactions.
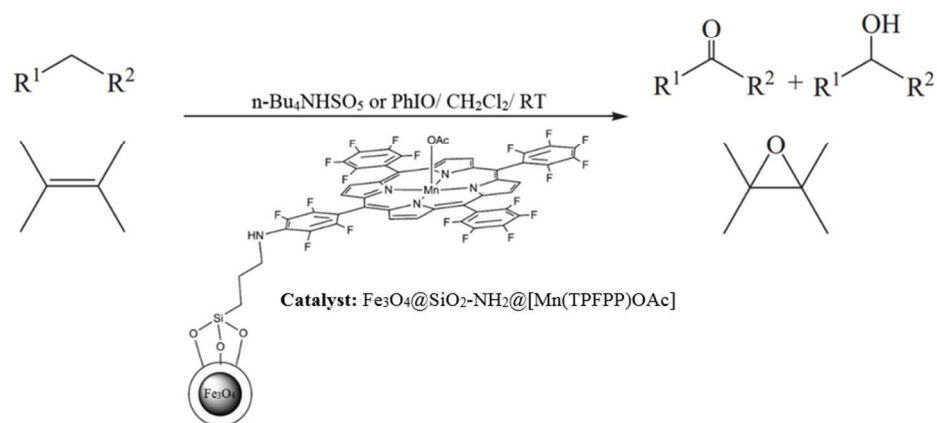
402 **Acknowledgments**

405

406

RSC Advances Accepted Manuscript

RSC Advances Accepted Manuscript

References

1 P. R. Ortiz de Montellano, *Cytochrome P450: Structure, Mechanism, and Biochemistry,* Plenum Press, New York, 2004.

2 D. Dolphin, T. G. Traylor and L. Y. Xie, *Acc. Chem. Res.,* 1997, **30**, 251-259.

3 J. P. Collman, X. Zhang, V. J. Lee, E. S. Uffelman and J. I. Brauman, *Science.,*1993, **261**, 1404-1411.

4 R. A. Sheldon and B. Meunier, *Biomimetic Oxidations Catalysed by Transition Metal Complexes,* Imperial College Press, London, 2000.

5 W. Nam, *Acc. Chem. Res.,* 2007, **40**, 522-531.

6 E. Brule and Y. R. De Miguel, *Org. Biomol. Chem.,* 2006, **4**, 599-609.

7 M. A. Schiavon, Y. Iamamoto, O. R. Nascimento and M. D. D. Assis, *J. Mol. Catal. A: Chem.,* 2001, **174**, 213-222.

8 N. Bizaia, E. H. de Faria, G. P. Ricci, P. S. Calefi, E. J. Nassar, K. A. D. F. Castro, S. Nakagaki, K. J. Ciuffi, R. Trujillano, M. A. Vicente, A. Gil and S. A. Korili, *ACS Appl. Mater. Interfaces,* 2009, **1**, 2667-2678.

9 A. K. Rahiman, S. Sreedaran, K. S. Bharathi and V. Narayanan, *J. Porous Mater.,* 2010, **17**, 711-718.

10 G. S. Machado, K. A. D. de Freitas Castro, F. Wypych and S. Nakagaki. *J. Mol. Catal. A: Chem.,* 2008, **283**, 99-107.

11 M. Halma, K. A. D. de Freitas Castro, V. Pre'vot, C. Forano, F. Wypych and S. Nakagaki. *J. Mol. Catal. A: Chem.,* 2009**, 310**, 42-50.

12 S. Evans and J. R. Lindsay Smith, *J. Chem. Soc., Perkin Trans. 2,* 2001, 174-180.

13 J. Safari and L. Javadian, *RSC Adv.,* 2014, **4**, 48973-48979.

14 N. Zohreh, S. H. Hosseini, A. Pourjavadi and C. Bennett, *RSC Adv.,* 2014, **4**, 50047-50055.

15 H. Keypour, M. Balali, M. M. Haghdoost and M. Bagherzadeh, *RSC Adv.,* 2015, **5**, 53349-53356.

16 S. Shylesh, W. R. Thiel and V. Schunemann, *Angew. Chem. Int. Ed.,* 2010, **49**, 3428-3459.

17 K. V. S. Ranganath, J. Kloesges, A. H. Schäfer and F. Glorius, *Angew. Chem. Int. Ed.,* 2010, **49**, 7786-7789.

18 K. V. S. Ranganath and F. Glorius, *Catal. Sci. Technol.,* 2011, **1**, 13-22.

19 M. Bagherzadeh and A. Mortazavi-Manesh, *J. Coord. Chem.,* 2015, **68**, 2347-2360.

20 A. Schätz, O. Reiser and W. J. Stark, *Chem. Eur. J.,* 2010, **16**, 8950-8967.

21 N. Saadatjoo, M. Golshekan, S. Shariati, H. Kefayati and P. Azizi, *J. Mol. Catal. A: Chem.,* 2013, **377**, 173-179.

22 H. Saltzman and J. G. Sharefkin, *Org. Synth. Coll.,* 1973, **5**, 658-663.

23 S. Compestrini and B. Meunier, *Inorg. Chem.,* 1992, **31**, 1999-2006.

437   24 A. S. Ivanova and A. I. Boldyrev, *Org. Biomol. Chem.,* 2014, **12**, 6145-6150.

438   25 J. S. Lindsey, I. C. Schreiman, H. C. Hsu, P. C. Kearney and A. M. Marguerettaz, *J. Org. Chem.,* 1987, **52**, 827-
439   836.

440   26 K. M. Kadish ,C. Araullo-McAdams, B. C. Han and M. M. Franzen, *J. Am. Chem. Soc.,* 1990, **112**, 8364-8368.

441   27 X. Q. Liu, Z. Y. Ma, J. M. Xing and H. Z. Liu, *J. Magn. Mater.,* 2004, **270**, 1-6.

442   28 M. Bagherzadeh, M. M. Haghdoost and A. Shahbazirad, *J. Coord. Chem.,* 2012, **65**, 591-601.

443   29 S. Campelj, D. Makovec and M. Drofenik, *J. Magn. Magn. Mater.,* 2009, **321**, 1346-1350.

444   30 M. Bagherzadeh, M. M. Haghdoost, F. Matlobi-Moghaddam, B. Koushki-Foroushani, S. Saryazdi and E. Payab,
445   *J. Coord. Chem.,* 2013, **66**, 3025-3036.

446   31 F. Wypych, A. Bail, M. Halma and Sh. Nakagaki, *J. Catal.,* 2005, **234**,431-437.

447   32 P. Battioni, J. F.Bartoli, D. Mansuy, Y. S. Byun and T. G. Traylor, *J. Chem. Soc. Chem. Commun.,* 1992, **15**,
448   1051-1053.

449   33 M. D. Assis and J. R. Lindsay Smith, *J. Chem. Soc., Perkin Trans. 2,* 1998, 2221-2226.

450   34 J. Wang, Q. W. Chen, C. Zeng and B. Y. Hou, *Adv. Mater.,* 2004, **16**, 137-140.

451   35 S. K. Walton, R. Q. Snurr, *J. Am. Chem. Soc.,* 2007, **129**, 8552–8556.

452   36 K. D. Kim, S. S. Kim, Y. H. Choa and H. T. Kim, *J. Ind. Eng. Chem.,* 2007, **13**, 1137-1141.

453   37 J. H. Cai, J. W. Huang, P. Zhao, Y. J. Ye, H. C. Yu and L. N. Ji, *J. Sol-Gel. Sci. Technol.,* 2009, **50**, 430-436.

454   38 C. Yuan, Z. Huang and J. Chen, *Catal. Lett.,* 2011, **141**,1484-1490.

455   39 P. Das, A. R. Silva, A. P. Carvalho, J. Pires and C. Freire, *J. Mater. Sci.,* 2009, **44**, 2865-2875.

456   40 Z. U. Rahman, Y. Dong, L. Su, Y. Ma, H. Zhang and X. Chen, *Chem. Eng. J.*, 2013, **222** 382-390.

457   41 M. Masteri-Farahani and N. Tayyebi, *J. Mol. Catal. A: Chem.,* 2011, **348**, 83-87.

458   42 Z. Gross and S. Ini, *J. Org. Chem.*, 1997, **62**, 5514-5521.

459   43 T. Matsui, S. Oyaki and Y. Watanabe, *J. Am. Chem. Soc.,* 1999, **121**, 9952-9957.

460   44 D. Mohajer, G. Karimipour and M. Bagherzadeh, *New J. Chem.,* 2004, **28**, 740-747.

461   45 A. Aghabali and N. Safari, *J. Porphyrins Phthalocyanines.,* 2010, **14**, 335-342.

462   46 J. L. McLain, J. Lee, J. T. Groves and B. Meunier, *Biomimetic Oxidations Catalyzed by Transition Metal*
463   *Complexes,* Imperial College Press, London, 2000, pp. 91-170.

464   47 C.-M. Che, V. K.-Y. Lo, C.-Y. Zhou and J.-S. Huang, *Chem. Soc. Rev.,* 2011, **40**, 1950-1975.

RSC Advances Accepted Manuscript

465 48 S. P. de Visser, W. Nam, in: K. M. Kadish, K. M. Smith, R. Guilard (Eds.), *Handbook of Porphyrin Science:*

466 *Catalysis and Bio-inspired Systems*, World Scientific Publishing, Singapore, 2010, pp. 85-140.

467 49 J. T. Groves, W. J. Kruper and R. C. Haushalter, *J. Am. Chem. Soc.,* 1980, **102**, 6375-6377.

468 50 R. J. Balahura, A. Sorokin, J. Bernadou and B. Meunier, *Inorg. Chem.,* 1997, **36**, 3488-3492.

469 51 J. Bernadou and B. Meunier, *Chem. Commun.,* 1998, **20**, 2167-2173.

470 52 J. A. Smegal and C. L. Hill, *J. Am. Chem. Soc.,* 1983, **105**, 3515-3521.

471 53 M. R. dos Santos, J. R. Diniz, A. M. Arouca, A. F. Gomes, F. C. Gozzo, S. M. Tamborim, A. L. Parize, P. A. Z.

472 Suarez and B. A. D. Neto, *ChemSusChem,* 2012, **5**, 716-726.

473 54 W. S. D. Silva, A. A. M. Lapis, P. A. Z. Suarez and B. A. D. Neto, *J. Mol. Catal. B: Enzym.,* 2011, **68**, 98-103.

474 55 P. A. Z. Suarez, M. S. C. Pereira, K. M. Doll, B. K. Sharma and S. Z. Erhan, *Ind. Eng. Chem. Res.,* 2009, **48**,

475 3268-3270.

476 56 P. Adao, J. C. Pessoa, R. T. Henriques, M. L. Kuznetsov, F. Avecilla, M. R. Maurya, U. Kumar and I. Correia,

477 *Inorg. Chem.,* 2009, **48**, 3542.

478 57 R. D. Arasasingham, G. X. He and T. C. Bruice*, J. Am. Chem. So*c., 1993, **115**, 7985-7991.

479 58 J. T. Groves and M. K. Stern, *J. Am. Chem. Soc.,* 1987, **109**, 3812-3814.

480 59 W. Nam, I. Kim, M. H. Lim, H. J. Choi, J. S. Lee and H. G. Jang, *Chem. Eur. J.*, 2002, **8**, 2067-2071.

481 60 T. G. Traylor, Y. Iamamoto and T. Nakano, *J. Am. Chem. Soc.* 1986, **108**, 3529-3531.

482 61 M. Amini, M. Bagherzadeh, Z. Moradi-Shoeili, D. M. Boghaei, A. Ellern and L. K. Woo*, J. Coord. Chem.,* 2013,

483 **66**, 464-472.

484 62 T. Heikkilä, R. Sillanpää and A. Lehtonen, *J. Coord. Chem.,* 2014, **67**, 1863-1872.

485 63 M. Amini, M. Bagherzadeh, B. Eftekhari-Sis, A. Ellern and L. K. Woo, *J. Coord. Chem.,* 2013, **66**, 1897-1905.

486 64 M. Bagherzadeh, M. Amini, A. Ellern and L. K. Woo, *Inorg. Chem. Commun.,* 2012, **15**, 52-55.

487 65 M. Zare, Z. Moradi–Shoeili, M. Bagherzadeh, S. Akbayrak and S. Özkar, *New J. Chem.,* 2015, **00**, 1-8.

488 66 S. Rayati, S. Zakavi, P. Jafarzadeh, O. Sadeghi and M. M. Amini, *J. Porphyrins Phthalocyanines.,* 2012, **16**, 260-

489 266.

490 67 S. Rayati, P. Jafarzadeh and S. Zakavi, *Inorg. Chem. Commun.,* 2013, **29**, 40-44.

270x144mm (96 x 96 DPI)